Structural and optoelectronic properties of ZnO:Al films with various thicknesses deposited by DC pulse magnetron sputtering

YING WANG[a,b*], WEIWEI JIANG[a,b], WANYU DING[a,b], YUN WANG[c], SHOU PENG[c], WEIPING CHAI[a,b]
[a]*School of Materials Science and Engineering, Dalian Jiaotong University, Dalian 116028, China*
[b]*Engineering Research Center of Optoelectronic Materials and Devices, Education Department of Liaoning Province, Dalian 116028, China*
[c]*State Key Laboratory of Advanced Technology for Float Glass, Bengbu 233018, China*

Transparent conductive ZnO:Al films with various thicknesses between 40 and 500 nm were deposited by direct current pulse magnetron sputtering at 270℃. The influence of film thickness on the crystal structure, surface morphology, optoelectronic properties was analyzed systematically. The crystal quality and the electrical properties of the films were improved with the increase of film thickness. The average transmittances in the visible region of all the films were over 90% regardless of film thickness. And the transmittance in the UV region decreased with increasing the film thickness. The grain size and roughness of films increased with the increasing film thickness.

(Received July 19, 2012; accepted October 30, 2012)

Keywords: ZnO:Al, Thin films, Optoelectronic materials, Thickness, Sputtering

1. Introduction

Transparent conducting oxide (TCO) films are under intense investigation and development for optoelectronic devices in recent years, such as solar cells, flat panel displays, liquid crystal displays, and light emitting diodes [1-4]. Indium tin oxide (ITO), SnO_2-based, and ZnO-based materials have been widely studied as typical TCO materials [5, 6]. Among these TCO materials, ZnO:Al (AZO) film is particularly attractive because of its excellent optoelectronic properties, non-toxicity, especially its low cost of manufacture and stability in hydrogen plasma environment [7-9]. In the past several years, many deposition methods have been used to prepare AZO films, including magnetron sputtering, pulsed laser deposition, chemical vapor deposition, spray pyrolysis, and sol-gel [10-14]. Among the above mentioned techniques, magnetron sputtering is considered to be a suitable technique due to its high deposition rate, good adhesion and controllability. The growth of sputtered AZO films is influenced by many factors such as substrate temperature, working pressure, deposition time, sputtering power, Ar flow rate, etc [15, 16]. The film thickness determined by deposition time, which is an important factor for the performance of optoelectronic devices, has considerable effects on the structure, surface morphology, and optoelectronic properties of AZO films. Thus, it is very important to investigate how the AZO film properties are affected by the film thickness.

In this paper, AZO thin films with thicknesses ranging from 40 to 500 nm were deposited on glass substrates by direct current (DC) pulse magnetron sputtering. The surface morphology and the structural, electrical and optical properties of AZO films with different thicknesses were investigated in detail.

2. Experimental

AZO films were deposited on glass substrates by DC pulse magnetron sputtering from an oxide ceramic target consisting of 98 wt.% ZnO and 2 wt.% Al_2O_3. After cleaning procedures, the substrate was loaded into the sputtering chamber. The base pressure of the sputtering chamber was 3×10^{-3} Pa. And then, Ar (99.999% in purity) was introduced into the chamber as sputtering gas. The working pressure during the process of deposition was kept at 0.8 Pa. Pre-sputtering for 5 min was adopted in order to clean the target surface. During the AZO films deposition, the substrate temperature and the sputtering power was fixed at 270℃ and 350 W, respectively. The AZO films with various thicknesses ranging from 40 to 500 nm were obtained by varying the deposition time.

The film thickness was measured by a Dektak 6M profilometer. The structural and crystalline properties of AZO films were analyzed by X-ray diffraction (XRD) using a PANalytical X'pert diffractometer with Cu

radiation. Atomic force microscope (AFM, Veeco DI-3100) was used to observe the surface morphology of AZO films. The optical properties of the AZO films were performed by using a U-3310 ultraviolet-visible spectrophotometer. The electrical properties were determined at room temperature by a Loresta EP MCP-T360 four-point probe.

3. Results and discussion

3.1 Structural properties

Fig. 1 shows the film thickness of AZO films as a function of deposition time. It can be seen that the thickness increases approximately linearly with the increasing deposition time. As shown in Fig. 1, the deposition rate is about 30 nm/min obtained from the linear fitting.

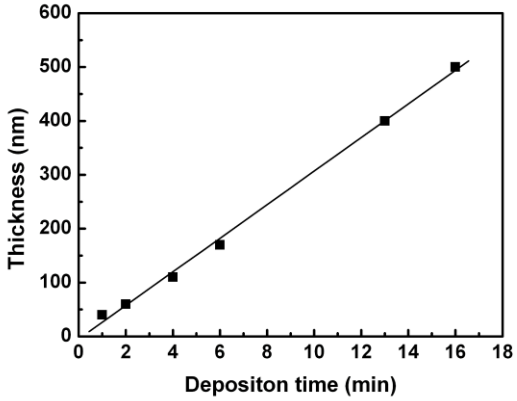

Fig. 1. Film thickness of AZO films as a function of deposition time.

Fig. 2 shows the XRD patterns of AZO films with different film thicknesses. All the films show a strong (002) diffraction peak at 2θ near 34º, which indicates that all the AZO films have a hexagonal wurtzite structure with c-axis preferred orientation to the surface of substrate [17]. A very weak diffraction peak near 72º, associated with (004) plane, is also observed. From the results, the dopant Al does not change the hexagonal wurtzite structure in the AZO films, and no Al_2O_3 characteristic peaks are observed. From Fig. 2, we can see clearly that the intensity of (002) peak increases rapidly with increasing the film thickness. And with the increase of film thickness, the position of (002) diffraction peak shifts toward high angle, which indicates that the lattice plane distance *d* decreases. As the films are deposited on amorphous glass, large stress exists in the thinner AZO films. However, for the thicker AZO films, the later deposited layer can form high quality texture easier on former AZO polycrystalline layer. So the stress in AZO films is reduced and the lattice plane distance *d* decreases with the increase of film thickness [18-20].

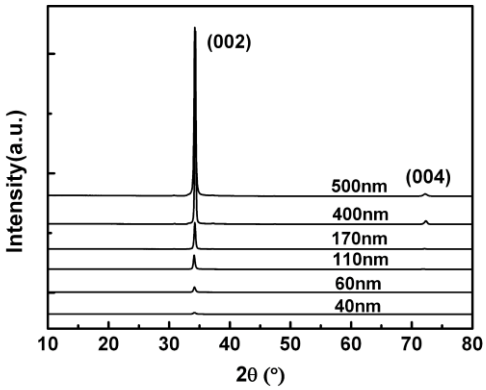

Fig. 2. XRD patterns of AZO films with different film thicknesses.

Table 1 lists the parameters about the (002) diffraction peak of AZO films with different film thicknesses.

The peak position shifts from 34.11º up to 34.22º with the increasing film thickness. The lattice plane distance *d* has been calculated using the Bragg formula. And the strains (ε) in the films are estimated by the following equation [21]:

$$\varepsilon = (c_{film} - c_{bulk})/c_{bulk} \qquad (1)$$

where c_{bulk} is the lattice constant of bulk ZnO (0.52069 nm) [22] and c_{film} is the lattice constant of AZO films. All the calculated results are shown in Table 1. The grain size (*D*) can be calculated by Scherrer formula [23]:

$$D = \frac{0.9\lambda}{\beta \cos\theta} \qquad (2)$$

where *D* is the grain size, λ is the X-ray wavelength, θ is the Bragg angle and β is the FWHM (full width at half maximum) of the AZO (002) diffraction peak. From the results, the grain size increases while the strain decreases as the film thickness increases.

Table 1. XRD results of AZO films with different film thicknesses: 2θ, lattice spacing d, grain size D and strain.

Film thickness (nm)	2θ (º)	***d* (nm)**	**Strain (%)**	***D* (nm)**
40	34.11	0.26271	0.908	18.117
60	34.14	0.26249	0.824	23.802
110	34.13	0.26256	0.851	29.520
170	34.20	0.26204	0.651	32.510
400	34.23	0.26182	0.565	42.008
500	34.22	0.26189	0.593	40.182

3.2 Surface morphology

The AFM morphological images of AZO films with different thicknesses are shown in Fig. 3. The surface morphology of films changes with the increasing film thickness gradually, which displays the film growth mode. It is clearly seen from Fig. 3 that the grain size increases with the increasing film thickness. During the initial processing of deposition, small grains appear. With the increasing deposition time, AZO columnar crystal forms gradually due to the low surface energy of (002) plane. AFM measurements are also used to determine the root mean square (RMS) roughness. The film thickness strongly influences the RMS roughness of deposited AZO films. The RMS roughness value increases from 1.163 to 4.483 nm when the film thickness increases from 40 to 500 nm.

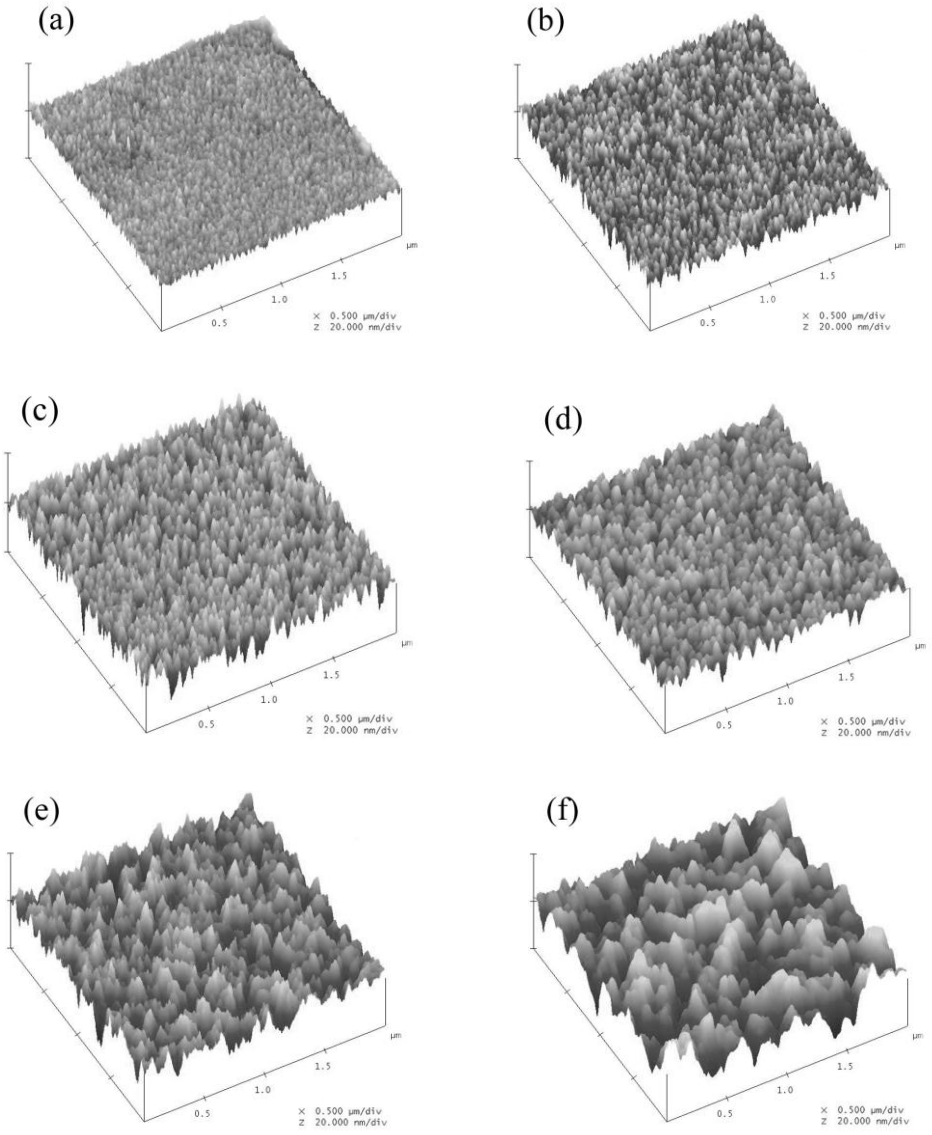

Fig. 3. AFM morphological images of AZO films with different film thicknesses: (a) 40 nm, (b) 60 nm, (c) 110 nm, (d) 170 nm, (e) 400 nm, (f) 500 nm.

3.3 Optical properties

Fig. 4 shows the optical transmittance in the wavelength range from 300 to 800 nm for AZO films with various thicknesses. As for applications in optoelectronic devices, the high optical transmittance in the visible region is indispensable for AZO films. In the wavelength range of 400-800 nm, the average transmittance for all AZO films is over 90%.

The energy in the UV region is higher than the band gap energy of AZO films, which results in the absorption of photon in the films [20]. The absorption of photon is

in dependence on the film thickness with the same incidence light. When the film is very thin, the absorption of photon will be limited in the films. So the optical transmittance does not disappear at the wavelength of 300 nm (larger than 0) for films thinner than 170 nm. And the transmittance in the UV region decreases obviously with the increase of film thickness. Furthermore, all the films exhibit an obvious absorption edge in the UV region. And the absorption edge shows a blue shift for the thinner films. From the XRD results, we can see that the grain size decreases with the decreasing film thickness. So the blue shift can be attributed to the smaller grains in the thinner film [24].

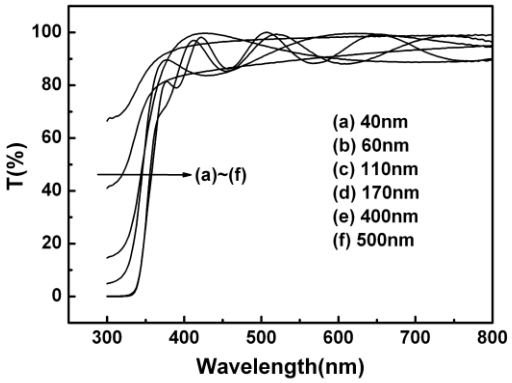

Fig. 4. Optical transmittance spectra of AZO films with different film thicknesses.

3.4 Electrical properties

The resistivity of AZO films as a function of film thickness is shown in Fig. 5. It can be seen that the resistivity decreases with the increase of film thickness, which indicates the electrical properties of AZO films are improved with the increasing film thickness. The 500 nm thick AZO film shows the lowest resistivity of about 1.4×10^{-3} Ω·cm. The changing trend of the resistivity can be interpreted by the following reasons. According to the formular $\rho = 1/nq\mu$, the resistivity (ρ) depends on the mobility (μ) and the carrier concentration (n) [25]. From the above AFM results, the grain size is smaller in the thinner films, which results in more grain boundary scattering. So the mobility for carrier is low. In addition, from the XRD results, large stress exists in the thinner films, which indicates that there are lots of defects in the films. These defects will act as the electron trap and cause the decrease of the carrier concentration. So the resistivity is higher in the thinner films. However, with increasing thickness of film, the formation of big grains results in the decrease of grain boundary scattering. Meanwhile, defects in the films are reduced. Thus, both mobility and carrier concentration increase, and the resistivity will decrease.

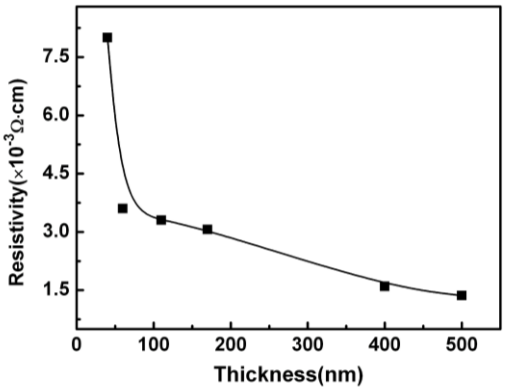

Fig. 5. Resistivity of AZO films as a function of film thickness.

4. Conclusions

In summary, AZO films with different film thicknesses were deposited on glass substrates at substrate temperature of 270℃ by DC pulse magnetron sputtering. All the AZO thin films showed a hexagonal wurtzite structure with a c-axis preferred orientation. With the increase of film thickness, the crystal quality of AZO film was improved and the value of (002) diffraction peak position increased due to the reduction of stress in the films. The grains size and RMS roughness increased when the film thickness was increased from 40 to 500 nm. All the AZO films had a high average transmittance of over 90% throughout the visible wavelength range. With the increasing film thickness, the transmittance in the UV region decreased obviously and the electrical properties of AZO films were improved. The 500 nm thick AZO film had the lowest resistivity of about 1.4×10^{-3} Ω·cm.

Acknowledgements

This work was supported by the National Natural Science Foundations of China (Grant No. 51002018 and 51102030), the Project of Open Research Foundation of the Ministry of Education Key Laboratory of Materials Modification (Dalian University of Technology) (Grant No. DP1050901), the Program for Liaoning Excellent Talents in University (Grant No. LJQ2011043), the Dalian Economy and Communication Committee Foundation of China (Grant No. 2009-3-215-jw-cxyhz), the Dalian Science and Technology Plan Projects of China (Grant No. 2010J21DW008 and 2011A15GX025) and the National Basic Research Program of China (Grant No. 2012CB724608).

References

[1] X. R. Deng, H. Deng, M. Wei, J. J. Chen, J. Mater. Sci. - Mater. Electron. **23**, 413 (2012).
[2] I. Akyuz, S. Kose, E. Ketenci, V. Bilgin, F. Atay, J. Alloys Compd. **509**, 1947 (2011).
[3] H. Liu, V. Avrutin, N. Izyumskaya, Ü. Özgür, H. Morkoç, Superlattices Microstruct. **48**, 458 (2010).
[4] I. Akyuz, S. Kose, F. Atay, V. Bilgin, Mater. Sci. Semicond. Process. **13**, 109 (2010).
[5] Hadj Benhebal, Messaoud Chaib, Angélique Leonard, Stéphanie D. Lambert, Michel Crine, Mater. Sci. Semicond. Process. **15**, 264 (2012).
[6] G. Cannella, F. Principato, M. Foti, C. Garozzo, S. Lombardo, Energy Procedia **3**, 51 (2011).
[7] F. Ruske, C. Jacobs, V. Sittinger, B. Szyszka, W. Werner, Thin Solid Films **515**, 8695 (2007).
[8] Y. H. Kim, K. S. Lee, T. S. Lee, B. K. Cheong, T. Y. Seong, W. M. Kim, Curr. Appl. Phys. **10**, S278 (2010).
[9] B. S. Chua, S. Xu, Y. P. Ren, Q. J. Cheng, K. Ostrikov, J. Alloys Compd. **485**, 379 (2009).
[10] J. I. Owen, W. D. Zhang, D. Köhl, J. Hüpkes, J. Cryst. Growth **344**, 12 (2012).
[11] X. Q. Gu, L. P. Zhu, L. Cao, Z. Z. Ye, H. P. He, Paul K. Chu, Mater. Sci. Semicond. Process. **14**, 48 (2011).
[12] D. Kim, I. Yun, H. Kim, Curr. Appl. Phys. **10**, S459 (2010).
[13] M. A. Kaid, A. Ashour, Appl. Surf. Sci. **253**, 3029 (2007).
[14] Y. S. Kim, W. P. Tai, Appl. Surf. Sci. **253**, 4911 (2007).
[15] H. Zhu, J. Hüpkes, E. Bunte, A. Gerber, S. M. Huang, Thin Solid Films **518**, 4997 (2010).
[16] Z. Y. Zhang, C. G. Bao, W. J. Yao, S. Q. Ma, L. L. Zhang, S. Z. Hou, Superlattices Microstruct. **49**, 644 (2011).
[17] S. Singh, R. S. Srinivasa, S. S. Major, Thin Solid Films **515**, 8718 (2007).
[18] S. Hayamizu, H. Tabata, H. Tanaka, T. Kawai, J. Appl. Phys. **80**, 787 (1996).
[19] B. Z. Dong, G. J. Fang, J. F. Wang, W. J. Guan, X. Z. Zhao, J. Appl. Phys. **101**, 33713 (2007).
[20] B. L. Zhu, S. J. Zhu, J. Wang, J. Wu, D. W. Zeng, C. S. Xie, Physica E **43**, 1738 (2011).
[21] M. Chen, Z. L. Pei, C. Sun, L. S. Wen, X. Wang, J. Cryst. Growth **220**, 254 (2000).
[22] S. J. Pearton, D. P. Norton, K. Ip, Y. W. Heo, T. Steiner, Prog. Mater. Sci. **50**, 293 (2005).
[23] L. Li, L. Fang, X. M. Chen, J. Liu, F. F. Yang, Q. J. Li, G.. B. Liu, S. J. Feng, Physica E **41**, 169 (2011).
[24] J. Yu, X. Zhao, Q. Zhao, Thin Solid Films **379**, 7 (2000).
[25] G.. J. Fang, D. J. Li, B. L. Yao, Thin Solid Films **418**, 156 (2002).

*Corresponding author: djtuwy@163.com